IEEE Transactions on Geoscience and Remote Sensing

Fourth Order Small Slope Theory of Sea Surface Brightness Temperatures

Journal:	*Transactions on Geoscience and Remote Sensing*
Manuscript ID:	TGRS-2006-00061
Manuscript Type:	Regular paper
Date Submitted by the Author:	13-Feb-2006
Complete List of Authors:	Demir, Metin Johnson, Joel
Keywords:	Rough surfaces, Radiometry, Emission

Transactions on Geoscience and Remote Sensing

Fourth Order Small Slope Theory of Sea Surface Brightness Temperatures

Metin A. Demir and Joel T. Johnson

Department of Electrical Engineering and ElectroScience Laboratory

The Ohio State University

205 Dreese Laboratories

2015 Neil Ave

Columbus, OH 43210

(614) 292-1593

ABSTRACT

A derivation of the fourth order term in the small slope approximation (SSA) of thermal emission from the sea surface is presented. It is shown that this term has the form of a four-fold integration over a product of two sea spectra for a Gaussian random process sea, thereby describing emission "interaction" effects among pairs of sea waves. An approximation for "long - long" wave interactions (i.e. the optical limit) is considered, and shown to match the physical optics theory. Interaction effects between "long" and "short" waves are also considered, both through numerical and approximate evaluations of the fourth order theory. The approximation developed has a form similar to an expanded "two-scale" model, and enables comparisons of short wave "tilting" effects between the two models in terms of spectrum independent "weighting" functions. The weighting functions obtained are found to be similar, but not identical, for the SSA and two-scale theories. In addition, azimuthal harmonics from the fourth order SSA expansion of long-short wave interactions for a particular sea surface model are compared against the full fourth order theory and the two-scale model. Results again show the SSA and two-scale models to yield similar, but not identical, predictions.

Keywords: rough surface scattering, microwave radiometry, thermal emission

1 Introduction

In recent years, models based on the small slope approximation (SSA) for emission from a rough surface have been applied to study sea surface brightness temperatures [1]-[4]. The formulation of these models is based on a small perturbation method (SPM) solution for scattering from a rough surface [5], which has been shown to yield a small slope theory when applied to the computation of surface emission [1]. One consequence of the small slope nature of the theory is the fact that the SSA model produces agreement with a physical optics (PO) theory for the contributions of large-scale waves when the PO theory is expanded in long-wave slope [6], while retaining agreement with SPM emission predictions for small scale surfaces.

The majority of previous studies have employed the second order SSA theory [1]-[2], either alone or in combination with a full geometrical optics approach to obtain a "two scale" model [7]-[8]. These second order SSA based theories predict that the influence of surface roughness on brightness temperatures can be expressed as an integration over the surface directional spectrum multiplied with an emission "weighting function" [2]. A third order SSA theory has also been derived recently [3]-[4], and obtains a correction to the second order results in terms of a quadruple integration over the surface bi-spectrum. Because the bi-spectrum vanishes identically for a surface described as a Gaussian random process, third order SSA results provide only limited information on the accuracy of second order predictions for a near-Gaussian process sea.

Extension of the theory to fourth order requires knowledge of the SPM scattering solution to fourth order. Explicit expressions up to second order in surface height were provided in [5]; explicit expressions up to third order have also been presented [9]. Reference [9] also presented a systematic procedure for determining fourth and higher order solutions, but the simplified results of this procedure were not provided. Recently, the systematic procedure described in [9] was applied to construct a recursive and arbitrary order solution [10] for scattered fields in the SPM method. This solution now enables formulation and evaluation of SSA emission contributions at fourth order.

One advantage of a fourth order model is its ability to capture emission "interactions" among multiple length scale waves in the sea surface. At second order, emission contributions from indi-

vidual sea waves are summed without regard to the presence of other waves. One major interaction neglected in this second order approach is the "tilting" of short waves by long waves that is included in a heuristic manner in the two scale theory. The fourth order SSA theory then should produce the first significant modeling of these effects for a near-Gaussian random process sea, and thereby enable comparisons with and evaluations of tilting effects included in the two-scale theory. The results to be presented here have been selected to provide an initial examination of this question.

In this paper, the SPM scattering solution of [10] is applied in Kirchhoff's Law of thermal emission [11] to derive the fourth order correction in the small slope emission theory. Section 2 briefly reviews the SPM scattering solution from [10] and introduces the notation to be utilized. These scattered field solutions are then applied in Section 3 with Kirchhoff's Law to derive the fourth order SSA emission term; it is shown that this term has the form of an integration over a product of two spectra for a Gaussian random process sea. In Section 4, the analysis of [6] is extended to fourth order to demonstrate again that the SSA theory continues to match a slope expanded PO theory for large-scale surface emission contributions.

Numerical evaluation of the 4-fold SSA4 integral for computing "long-short" wave interactions is discussed in Section 5, and an approximation for computing such interactions is presented in Section 6. The form of the approximation obtained allows a sea spectrum independent comparison with the two-scale theory of long-short wave tilting effects to be performed in terms of a set of weighting functions; these functions are found to be similar but not identical between the two theories. To provide more concrete illustrations, Section 7 presents azimuthal harmonic coefficients of emitted brightnesses obtained from numerical 4-fold SSA4 integration and compares with predictions of the approximation from Section 6 as well as the two-scale theory. Results show the SSA4 expansion to perform well for computing long-short wave interactions, and that SSA4 and two-scale model predictions remain similar but not identical. Final discussions and conclusions are provided in Section 8.

2 Review of SPM scattered field solution

The basic notation introduced in [9]-[10] is used below unless otherwise notated. Consider a periodic rough interface $z = f(x, y)$ separating free space ($z > f(x, y)$) from a dielectric region with relative permittivity ϵ. A plane wave is incident from free space upon this interface; the resulting scattered and transmitted fields can be completely described in terms of the polarization complex amplitudes of a set of Floquet modes. Horizontally and vertically polarized scattered mode complex amplitudes are denoted by $\alpha_{\overline{n}'}$ and $\beta_{\overline{n}'}$, respectively, while $\gamma_{\overline{n}'}$ and $\delta_{\overline{n}'}$ refer to transmitted horizontally and vertically polarized complex amplitudes, respectively. Here $\overline{n}' = (n', m')$ provides indexes to a particular Floquet mode, thus describing the direction of propagation of the corresponding scattered or transmitted field. Note the requirement for a periodic interface can be removed after the solution is completed by allowing the periods to approach infinity, as in [5].

Following the process in [9] but shifting some of the indices appropriately allows the multiple terms in [9] to be combined. Scattering and transmission coefficients, all united in a vector quantity, $\bar{\zeta} = [\alpha, \beta, \gamma, \delta]^T$ at Nth order ($N \geq 2$) can then be expressed as [10]:

$$\begin{aligned} \bar{\zeta}^{(N)}_{\overline{n}'} &= \sum_{\overline{n}_1} \sum_{\overline{n}_2} \cdots \sum_{\overline{n}_{N-1}} h_{\overline{n}_1} h_{\overline{n}_2} \ldots h_{\overline{n}_{N-1}} h_{\overline{n}'-\overline{n}_1-\cdots\overline{n}_{N-1}} \\ &\quad \cdot \bar{g}^{(N)}\left(\overline{n}', \overline{n}_1, \ldots, \overline{n}_{N-1}\right) \end{aligned} \tag{1}$$

where $h_{\overline{n}}$ refers to the Fourier coefficients of the surface; note N of these are included so that the overall term is Nth order in surface height. The Nth order SPM "kernel" is expressed in terms of lower order kernels as follows [10]:

$$\begin{aligned} \bar{g}^{(N)}\left(\overline{n}', \overline{n}_1, \ldots, \overline{n}_{N-1}\right) &= \bar{g}^{(N,0)}\left(\overline{n}', \overline{n}_1, \ldots, \overline{n}_{N-1}\right) \\ &\quad + \sum_{l=1}^{N-1} \left[\bar{\bar{\nu}}^{(N-l)}\left(\overline{n}', \overline{n}_s^{(l)}, \overline{n}_{l+1}, \ldots, \overline{n}_{N-1}\right) \right. \\ &\quad \left. \cdot \bar{g}^{(l)}\left(\overline{n}_s^{(l)}, \overline{n}_2, \ldots, \overline{n}_l\right) \right] \end{aligned} \tag{2}$$

where $\overline{n}_s^{(l)}$ is

$$\overline{n}_s^{(l)} = \sum_{i=1}^{l} \overline{n}_i \tag{3}$$

The $\bar{\bar{\nu}}^{(N-l)}(\overline{n}', \overline{n}, \overline{n}_1, \ldots, \overline{n}_{N-l-1})$ quantity above is a four-by-four tensor with elements ν_{ij} at row i and column j, while the kernel function vector $\bar{g}^{(l)}$ for $l = 1$ to N is a 4 element column vector defined analogously to $\bar{\zeta}$. Elements of the $\bar{\bar{\nu}}^{N-l}$ tensor, the $\bar{g}^{(N,\,0)}$ quantity, and other details are given in [10]. The above formulation provides a recursive solution that is easily programmed for determining the SPM kernel at a specific argument and at arbitrary order.

Note that ultimately the transmission coefficients (γ, δ) of $\bar{\zeta}$ are not needed when computing thermal emission (the SSA theory is known to conserve power at a given order), so only the scattering coefficients are of interest in what follows. We introduce a revised notation to simplify consideration of polarimetric emission by defining $f^{(N)}_{qp,\overline{n}'}$ as the complex amplitude of the Floquet mode indexed by $\overline{n}'$ at Nth order in scattered polarization q for incident polarization p, with p and q chosen from h or v for horizontal and vertical, respectively. For example, $f^{(N)}_{hh,\overline{n}'}$ would be defined as $\alpha^{(N)}_{\overline{n}'}$ for a horizontally polarized incident plane wave, with $\alpha^{(N)}_{\overline{n}'}$ representing the first row of the $\bar{\zeta}^{(N)}_{\overline{n}'}$ vector in Equation (1). Similarly we adopt the notation $g^{(N)}_{qp,\overline{n}'}$ for the Nth order SPM kernel function corresponding to $f^{(N)}_{hh,\overline{n}'}$. This notational modification is necessary due to the fact that Equation (1) must be considered separately for horizontal and vertical incident polarizations.

3 Fourth order emission theory

Kirchhoff's Law requires computation of the total surface reflectivity in order to determine surface emissivity. The total surface reflectivity is determined by integrating the total power scattered into the upper hemisphere under plane wave illumination. Furthermore, appropriate combinations of polarization coefficients [11] must be considered in order to compute polarimetric brightnesses. For a periodic surface, plane wave illumination results in a large set of Floquet modes scattered bistatically above the surface. The complex amplitude of each of these modes is expressed as a series up to fourth order in the SPM solution. Computation of the power in a given mode then results in a corresponding series for the scattered power in that mode up to fourth order. The fourth order contribution to the total surface reflectivity is then determined by adding (or integrating in the continuous surface limit) all fourth order power contributions from each scattered mode.

Following this process, the fourth order contribution of the Floquet mode indexed by $\overline{n}'$ to the total surface reflectivity in a given polarimetric quantity can be written as

$$\begin{aligned}
P^{(4)}_{h,\overline{n}'} &= 2\mathrm{Re}\Big\{ f^{(0)}_{hh} f^{(4)*}_{hh} + f^{(0)}_{vh} f^{(4)*}_{vh} \\
&\quad + \mathrm{Re}\left\{ \frac{k_{z,\overline{n}'}}{k_{zi}} \right\} \left(f^{(1)}_{hh} f^{(3)*}_{hh} + f^{(1)}_{vh} f^{(3)*}_{vh} \right) \Big\} \\
&\quad + \mathrm{Re}\left\{ \frac{k_{z,\overline{n}'}}{k_{zi}} \right\} \left(|f^{(2)}_{hh}|^2 + |f^{(2)}_{vh}|^2 \right) \qquad (4) \\
P^{(4)}_{v,\overline{n}'} &= 2\mathrm{Re}\Big\{ f^{(0)}_{vv} f^{(4)*}_{vv} + f^{(0)}_{hv} f^{(4)*}_{hv} \\
&\quad + \mathrm{Re}\left\{ \frac{k_{z,\overline{n}'}}{k_{zi}} \right\} \left(f^{(1)}_{vv} f^{(3)*}_{vv} + f^{(1)}_{hv} f^{(3)*}_{hv} \right) \Big\} \\
&\quad + \mathrm{Re}\left\{ \frac{k_{z,\overline{n}'}}{k_{zi}} \right\} \left(|f^{(2)}_{vv}|^2 + |f^{(2)}_{hv}|^2 \right) \qquad (5) \\
P^{(4)}_{U,\overline{n}'} &= 2\mathrm{Re}\Big\{ f^{(0)}_{vv} f^{(4)*}_{vh} + f^{(4)}_{hv} f^{(0)*}_{hh} \\
&\quad + \mathrm{Re}\left\{ \frac{k_{z,\overline{n}'}}{k_{zi}} \right\} \Big(f^{(1)}_{vv} f^{(3)*}_{vh} + f^{(2)}_{vv} f^{(2)*}_{vh} + f^{(3)}_{vv} f^{(1)*}_{vh} \\
&\quad + f^{(1)}_{hv} f^{(3)*}_{hh} + f^{(2)}_{hv} f^{(2)*}_{hh} + f^{(3)}_{hv} f^{(1)*}_{hh} \Big) \Big\} \qquad (6) \\
P^{(4)}_{V,\overline{n}'} &= 2\mathrm{Im}\Big\{ f^{(0)}_{vv} f^{(4)*}_{vh} + f^{(4)}_{hv} f^{(0)*}_{hh} \\
&\quad + \mathrm{Re}\left\{ \frac{k_{z,\overline{n}'}}{k_{zi}} \right\} \Big(f^{(1)}_{vv} f^{(3)*}_{vh} + f^{(2)}_{vv} f^{(2)*}_{vh} + f^{(3)}_{vv} f^{(1)*}_{vh} \\
&\quad + f^{(1)}_{hv} f^{(3)*}_{hh} + f^{(2)}_{hv} f^{(2)*}_{hh} + f^{(3)}_{hv} f^{(1)*}_{hh} \Big) \Big\} \qquad (7)
\end{aligned}$$

Here $*$, Re, and Im denote the complex conjugate, real, and imaginary part operators, respectively. The subscript $\overline{n}'$ is omitted above on the f quantities for simplicity, and the quantity $k_{zi} = k_0 \cos\theta_i$ is related to the radiometer polar observation angle θ_i, with k_0 the electromagnetic wavenumber. The quantity $k_{z,\overline{n}'}$ refers to the z component of the vector wavenumber of the Floquet mode indexed by $\overline{n}'$, as defined in [9]. Finally, the subscripts h, v, U, and V of the P quantities refer to the horizontal, vertical, U, and V polarimetric radiometer channels, respectively. The above expressions are to be summed over all propagating modes (i.e. all values of $\overline{n}'$ corresponding to propagating Floquet modes.)

When the SPM solution for the $f^{(N)}_{qp,\overline{n}'}$ complex amplitudes from Equation (1) is substituted

into the above and summed over $\overline{n}'$, a combination of sums over surface Fourier coefficients and SPM kernel functions results for determining $R_\zeta^{(4)}$, the total surface reflectivity. By shifting indices within these sums, it is possible to combine the multiple terms in this combination into a single "emission kernel" multiplying a single set of surface Fourier coefficients:

$$\begin{aligned} R_\zeta^{(4)} &= \sum_{\overline{n}_1}\sum_{\overline{n}_2}\sum_{\overline{n}_3} h_{\overline{n}_1} h_{\overline{n}_2} h_{\overline{n}_3} h_{-\overline{n}_1-\overline{n}_2-\overline{n}_3} \\ &\qquad \cdot g_\zeta^{T,(4)}(\overline{n}_1,\overline{n}_2,\overline{n}_3) \end{aligned} \tag{8}$$

Here ζ refers to h, v, U, or V, while $g_\zeta^{T,(4)}$ is the new reflectivity kernel obtained in this process. The resulting kernel for the horizontal reflectivity is

$$\begin{aligned} g_h^{T,(4)} &= \mathrm{Re}\left\{\frac{k_{z(\overline{n}_1+\overline{n}_3)}}{k_{zi}}\right\}\cdot \\ &\quad \Big(g_{hh}^{(2)}(\overline{n}_1+\overline{n}_3,\overline{n}_1)\; g_{hh}^{(2)*}(\overline{n}_1+\overline{n}_3,-\overline{n}_2) \\ &\quad + g_{vh}^{(2)}(\overline{n}_1+\overline{n}_3,\overline{n}_1)\; g_{vh}^{(2)*}(\overline{n}_1+\overline{n}_3,-\overline{n}_2)\Big) \\ &\quad +2\mathrm{Re}\Bigg\{\Gamma_h^*\; g_{hh}^{(4)}(\overline{0},\overline{n}_1,\overline{n}_2,\overline{n}_3) \\ &\qquad + \mathrm{Re}\left\{\frac{k_{z(-\overline{n}_3)}}{k_{zi}}\right\}\cdot \\ &\quad \Big(g_{hh}^{(1)*}(-\overline{n}_3)\; g_{hh}^{(3)}(-\overline{n}_3,\overline{n}_1,\overline{n}_2) \\ &\quad + g_{vh}^{(1)*}(-\overline{n}_3)\; g_{vh}^{(3)}(-\overline{n}_3,\overline{n}_1,\overline{n}_2)\Big)\Bigg\} \end{aligned} \tag{9}$$

where Γ_h is used to notate the horizontally polarized Fresnel reflection coefficient (as in [9]). The notation $k_{z,\overline{n}}$ again is utilized to indicate the z component of the vector wavenumber of the Floquet mode indexed by $\overline{n}$. The vertical reflectivity kernel $g_v^{T,(4)}$ can easily be obtained from the previous expression by interchanging the subscripts h and v.

The third Stokes' parameter reflectivity kernel is

$$g_U^{T,(4)} = 2\mathrm{Re}\Big\{\Gamma_v\; g_{vh}^{(4)*}(\overline{0},-\overline{n}_1,-\overline{n}_2,-\overline{n}_3)$$

$$
\begin{aligned}
&+ \Gamma_h^* \; g_{hv}^{(4)}(\overline{0}, \overline{n}_1, \overline{n}_2, \overline{n}_3) \\
&+ \mathrm{Re}\left\{ \frac{k_{z(\overline{n}_3)}}{k_{zi}} \right\} \cdot \\
&\Big(g_{hv}^{(1)}(\overline{n}_3) \; g_{hh}^{(3)*}(\overline{n}_3, -\overline{n}_1, -\overline{n}_2) \\
&+ g_{vv}^{(1)}(\overline{n}_3) \; g_{vh}^{(3)*}(\overline{n}_3, -\overline{n}_1, -\overline{n}_2) \Big) \\
&+ \mathrm{Re}\left\{ \frac{k_{z(\overline{n}_1+\overline{n}_3)}}{k_{zi}} \right\} \cdot \\
&\Big(g_{hv}^{(2)}(\overline{n}_1+\overline{n}_3, \overline{n}_1) \; g_{hh}^{(2)*}(\overline{n}_1+\overline{n}_3, -\overline{n}_2) \\
&+ g_{vv}^{(2)}(\overline{n}_1+\overline{n}_3, \overline{n}_1) \; g_{vh}^{(2)*}(\overline{n}_1+\overline{n}_3, -\overline{n}_2) \Big) \\
&+ \mathrm{Re}\left\{ \frac{k_{z(-\overline{n}_3)}}{k_{zi}} \right\} \cdot \\
&\Big(g_{hv}^{(3)}(-\overline{n}_3, \overline{n}_1, \overline{n}_2) \; g_{hh}^{(1)*}(-\overline{n}_3) \\
&+ g_{vv}^{(3)}(-\overline{n}_3, \overline{n}_1, \overline{n}_2) \; g_{vh}^{(1)*}(-\overline{n}_3) \Big) \Bigg\}
\end{aligned} \tag{10}
$$

The fourth Stokes' parameter brightness kernel $g_V^{T,(4)}$ is obtained by replacing the Re operator at the beginning of Equation (10) with the Im operator.

If an ensemble average over a stochastic surface process is taken in Equation (8), the surface statistic of interest is

$$< h_{\overline{n}_1} h_{\overline{n}_2} h_{\overline{n}_3} h_{-\overline{n}_1-\overline{n}_2-\overline{n}_3} > \tag{11}$$

where the $< \cdot >$ notation refers to an ensemble average. In the continuous surface limit (i.e. as the surface periods approach infinity [5]), the fourth order reflectivity correction has the form of a six-fold integration:

$$
\begin{aligned}
&\int\int d\mathbf{k}_1 \int\int d\mathbf{k}_2 \int\int d\mathbf{k}_3 \\
&\quad T(\mathbf{k}_1, \mathbf{k}_2, \mathbf{k}_3) g_\zeta^{T,(4)}(\mathbf{k}_1, \mathbf{k}_2, \mathbf{k}_3)
\end{aligned} \tag{12}
$$

Here $\mathbf{k}$ represents the (k_x, k_y) couple and the integration limits are infinite. The previous ensemble averaged quantity is now expressed as T, which is the fourth moment of the random rough surface,

given in terms of surface spectra W as follows:

$$\begin{aligned} T &= W(\mathbf{k}_1)W(\mathbf{k}_2)\delta(\mathbf{k}_3+\mathbf{k}_2) \\ &\quad +W(\mathbf{k}_1)W(\mathbf{k}_2)\delta(\mathbf{k}_3+\mathbf{k}_1) \\ &\quad +W(\mathbf{k}_3)W(\mathbf{k}_{22})\delta(\mathbf{k}_1+\mathbf{k}_2)+T_{tri} \end{aligned} \tag{13}$$

The quantity T_{tri} is the surface tri-spectrum, which describes non-Gaussian sea surface properties at fourth order. However little empirical information is available on the sea surface tri-spectrum, making its further consideration difficult at this point in time.

For a Gaussian random process (GRP), the tri-spectrum (T_{tri}) vanishes, and the Dirac delta functions can be utilized in Equation (12) to obtain a four-fold integration for the fourth order brightness correction

$$\begin{aligned} \Delta T_\gamma^{(4)} &= -T_s \int dk_x \int dk_y \int dk'_x \int dk'_y W(k_x,k_y) \\ &\quad W(k'_x,k'_y) g_\zeta^{T,(4),shf}(k_x,k_y,k'_x,k'_y) \end{aligned} \tag{14}$$

where T_s is the surface physical temperature, and a modified kernel is used:

$$g_\zeta^{T,(4),shf}(\mathbf{k}_1,\mathbf{k}_2) = g_\zeta^{T,(4)}(\mathbf{k}_1,-\mathbf{k}_1,\mathbf{k}_2) + g_\zeta^{T,(4)}(\mathbf{k}_1,\mathbf{k}_2,-\mathbf{k}_1) + g_\zeta^{T,(4)}(\mathbf{k}_1,\mathbf{k}_2,-\mathbf{k}_2) \tag{15}$$

The integration limits above are again infinite.

Equation (14) presents the final form of the fourth order brightness correction to be utilized in the remainder of this paper. Note this form couples contributions from sea waves at distinct sea wavenumbers (i.e. (k_x,k_y) and (k'_x,k'_y)) so that emission "interaction" effects among two sea waves are included. The superscript shf will typically be omitted on the kernel functions in what follows for simplicity.

4 Reduction to the optical limit

The first examination of Equaton (14) to be performed involves its properties for computing interactions among pairs of "long" waves. The SSA4 theory is expected to reduce to a slope expansion of the physical optics theory in this limit, as has been shown previously [6]. Here the analysis is

continued to fourth order to provide a complete verification, as well as a test of the SSA4 theory derivation.

4.1 "Long-long" wave expansion of SSA4 contributions

Coupling between pairs of "long" waves in Equation (14) implies that the region of interest in the integration domain lies near the origin of the four dimensional space. A Taylor expansion of the kernel functions about the origin to fourth order produces seventy terms, most of which vanish or are canceled by other terms in the Taylor expansion. The remaining non-zero fourth-order derivatives are multiplied by polynomial functions in k_x, k_y, k'_x, or k'_y, which allow the integrations over the spectra to be performed and result in double combinations of second order surface slope moments. The final form for the obtained brightnesses is

$$\begin{aligned}\Delta T_\zeta^{(4)} \approx -T_s \Bigg(& \begin{bmatrix} \frac{1}{4}\left(g^{T,(4)}_{\zeta,(k_x)^2,(k'_x)^2} < S_x^2 >^2 + g^{T,(4)}_{\zeta,(k_y)^2,(k'_y)^2} < S_y^2 >^2\right) \\ \frac{1}{2}\left(g^{T,(4)}_{\zeta,(k_x)^2,k'_x,k'_y} + g^{T,(4)}_{\zeta,k_x,k_y,(k'_x)^2}\right) < S_x^2 >< S_x S_y > \end{bmatrix} \\ & + \begin{bmatrix} \frac{1}{4}\left(g^{T,(4)}_{\zeta,(k_x)^2,(k'_y)^2} + g^{T,(4)}_{\zeta,(k_y)^2,(k'_x)^2}\right) < S_x^2 >< S_y^2 > \\ \frac{1}{2}\left(g^{T,(4)}_{\zeta,(k_y)^2,k'_x,k'_y} + g^{T,(4)}_{\zeta,k_x,k_y,(k'_y)^2}\right) < S_x S_y >< S_y^2 > \end{bmatrix} \\ & + \begin{bmatrix} g^{T,(4)}_{\zeta,k_x,k_y,k'_x,k'_y} < S_x S_y >^2 \\ 0 \end{bmatrix} \Bigg) \end{aligned} \tag{16}$$

In the vector notation here (identical to [6]), the first row represents the horizontal and vertical polarizations, while the second row is for the third and fourth Stokes' parameters. The additional subscripts on the $g_\zeta^{T,(4)}$ quantities refer to the particular fourth order derivative in the Taylor series expansion of the original $g_\zeta^{T,(4)}$ function about the origin. Following [6], $< S_x^2 >$ and $< S_y^2 >$ are the large-scale surface slope variances along and perpendicular the radiometer look direction, respectively. This choice implies that the brightness kernels are evaluated with the radiometer azimuthal observation angle set to 0 degrees.

The slope moments in Equation (16) can be expressed in terms of up and cross wind slope variances $< S_u^2 >$ and $< S_c^2 >$ as follows:

$$\begin{aligned} < S_x^2 >^2 &= \frac{1}{8}\left[S_1^4 + 4\ S_2^4\ \cos(2\phi_w) + S_3^4\ \cos(4\phi_w)\right] \\ < S_y^2 >^2 &= \frac{1}{8}\left[S_1^4 - 4\ S_2^4\ \cos(2\phi_w) + S_3^4\ \cos(4\phi_w)\right] \end{aligned}$$

$$
\begin{aligned}
< S_x S_y >^2 &= \frac{1}{8}\left[S_3^4 - S_3^4 \cos(4\phi_w)\right] \\
< S_x^2 >< S_y^2 > &= \frac{1}{8}\left[S_4^4 - S_3^4 \cos(4\phi_w)\right] \\
< S_x^2 >< S_x S_y > &= -\frac{1}{8}\left[2\, S_2^4 \sin(2\phi_w) + S_3^4 \sin(4\phi_w)\right] \\
< S_x S_y >< S_y^2 > &= -\frac{1}{8}\left[2\, S_2^4 \sin(2\phi_w) - S_3^4 \sin(4\phi_w)\right]
\end{aligned} \tag{17}
$$

where S_1^4, S_2^4, S_3^4, and S_4^4 are defined as:

$$
\begin{aligned}
S_1^4 &= 3 < S_u^2 >^2 + 2 < S_u^2 >< S_c^2 > + 3 < S_c^2 >^2 \\
S_2^4 &= < S_u^2 >^2 - < S_c^2 >^2 \\
S_3^4 &= < S_u^2 >^2 - 2 < S_u^2 >< S_c^2 > + < S_c^2 >^2 \\
S_4^4 &= < S_u^2 >^2 + 6 < S_u^2 >< S_c^2 > + < S_c^2 >^2
\end{aligned} \tag{18}
$$

and it is assumed that the radiometer look direction (i.e. the x axis) makes an angle ϕ_w with respect to the wind direction.

The azimuthal dependence of the fourth order long wave contributions in the optical limit then can be written explicitly as:

$$
\begin{aligned}
\Delta T_\zeta^{(4)} \approx & -T_s \left(\begin{bmatrix} \frac{1}{32} S_1^4 \left[g^{T,(4)}_{\zeta,(k_x)^2,(k'_x)^2} + g^{(T,4)}_{\zeta,(k_y)^2,(k'_y)^2} + g^{T,(4)}_{\zeta,(k_x)^2,(k'_y)^2} + g^{T,(4)}_{\zeta,(k_y)^2,(k'_x)^2} \right] \\ 0 \end{bmatrix} \right. \\
& + \begin{bmatrix} \frac{1}{8} S_2^4 \left[g^{T,(4)}_{\zeta,(k_x)^2,(k'_x)^2} - g^{T,(4)}_{\zeta,(k_y)^2,(k'_y)^2} \right] \cos(2\phi_w) \\ -\frac{1}{8} S_2^4 \left[\left(g^{T,(4)}_{\zeta,(k_x)^2,k'_x,k'_y} + g^{T,(4)}_{\zeta,k_x,k_y,(k'_x)^2} \right) + \left(g^{T,(4)}_{\zeta,(k_y)^2,k'_x,k'_y} + g^{T,(4)}_{\zeta,k_x,k_y,(k'_y)^2} \right) \right] \sin(2\phi_w) \end{bmatrix} \\
& \left. + \begin{bmatrix} \frac{1}{32} S_3^4 \left[g^{T,(4)}_{\zeta,(k_x)^2,(k'_x)^2} + g^{T,(4)}_{\zeta,(k_y)^2,(k'_y)^2} - 3 \left(g^{T,(4)}_{\zeta,(k_x)^2,(k'_y)^2} + g^{T,(4)}_{\zeta,(k_y)^2,(k'_x)^2} \right) \right] \cos(4\phi_w) \\ -\frac{1}{16} S_3^4 \left[\left(g^{T,(4)}_{\zeta,(k_x)^2,k'_x,k'_y} + g^{T,(4)}_{\zeta,k_x,k_y,(k'_x)^2} \right) - \left(g^{T,(4)}_{\zeta,(k_y)^2,k'_x,k'_y} + g^{T,(4)}_{\zeta,k_x,k_y,(k'_y)^2} \right) \right] \sin(4\phi_w) \end{bmatrix} \right) \\
\approx & -T_s \left(S_1^4 \; L^4_{\zeta,0}(\theta_i,\epsilon) + S_2^4 \; L^4_{\zeta,2}(\theta_i,\epsilon) \begin{bmatrix} \cos(2\phi_w) \\ \sin(2\phi_w) \end{bmatrix} \right. \\
& \left. + S_3^4 \; L^4_{\zeta,4}(\theta_i,\epsilon) \begin{bmatrix} \cos(4\phi_w) \\ \sin(4\phi_w) \end{bmatrix} \right)
\end{aligned} \tag{19}
$$

The fact that $g^{T,(4)}_{\zeta,(k_x)^2,(k'_y)^2} + g^{T,(4)}_{\zeta,(k_y),(k'_x)^2} = 2 g^{T,(4)}_{\zeta,k_x,k_y,k'_x,k'_y}$ is used in obtaining this expression.

The final form for long wave contributions at fourth order (Equation (19)) is similar to the forms at second and third order [6], and shows the presence of zeroth, second, and fourth azimuthal

harmonics in the emission signatures for a Gaussian process sea. Surface effects are described only in terms of the long wave slope moments, as is typical in the optical limit, while emission effects are captured entirely by a set of "long wave functions" $L^4_{\zeta,k}$. The latter depend only on the observation angle and the surface permittivity.

Note that the slope factors that scale the long wave functions for distinct emission azmiuthal variations (i.e. $k = 0, 2,$ or 4) are likely to be significantly different for the sea surface: the zeroth harmonic term S^4_1 is a function only of the sum of the along and cross-wind slope variances, while S^4_2 which scales the second azimuthal harmonic involves a product of the sum and difference of the along and cross wind slope variances. The fourth harmonic slope factor S^4_3 finally is the square of the difference between the up and cross wind slope variances. Because differences between the up and cross wind slope variances for the sea surface are typically small, these facts indicate that fourth azimuthal harmonics should generally be much smaller than the corresponding zeroth and second azimuthal harmonics.

4.2 Fourth order expansion of physical optics theory

In the physical optics theory, brightness temperatures can be written as a double integration over the slope pdf [6]:

$$T_\zeta \;=\; T_s \int_{-\infty}^{\infty} d\alpha \int_{-\infty}^{\infty} d\beta \; g^{PO}_\zeta(\alpha,\beta)\; f(\alpha,\beta) \tag{20}$$

where the PO kernel function g^{PO}_ζ is described in [6]. Using a Taylor expansion of the PO kernel $g^{PO}_\zeta(\alpha,\beta)$ about the origin and considering only the fourth order terms produces:

$$\Delta T^{PO,(4)}_\zeta \;\approx\; -T_s \left[\begin{array}{c} \frac{1}{24}\left(g^{PO}_{\zeta,(\alpha)^4} < S^4_x > + g^{PO}_{\zeta,(\beta)^4} < S^4_y >\right) + \frac{1}{4}\left(g^{PO}_{\zeta,(\alpha)^2,(\beta)^2} < S^2_x\; S^2_y >\right) \\ \frac{1}{6}\left(g^{PO}_{\zeta,(\alpha)^3,\beta} < S^3_x\; S_y > + g^{PO}_{\zeta,\alpha,(\beta)^3} < S_x\; S^3_y >\right) \end{array} \right] \tag{21}$$

Sea surface fourth order slope moments can be expressed in terms of up and cross wind moments $< S^4_u >$, $< S^2_u\; S^2_c >$ and $< S^4_c >$ as follows:

$$\begin{aligned} < S^4_x > \;=\; & \frac{3}{8}\left[< S^4_u > + 2\; < S^2_u\; S^2_c > + < S^4_c >\right] \\ & + \frac{1}{2}\left[< S^4_u > - < S^4_c >\right] \cos 2\phi_w \\ & + \frac{1}{8}\left[< S^4_u > - 6\; < S^2_u\; S^2_c > + < S^4_c >\right] \cos 4\phi_w \end{aligned} \tag{22}$$

$$
\begin{aligned}
< S_x^3\ S_y > &= -\frac{1}{4}\left[< S_u^4 > - < S_c^4 >\right]\sin 2\phi_w \\
&\quad -\frac{1}{8}\left[< S_u^4 > -6 < S_u^2 S_c^2 > + < S_c^4 >\right]\sin 4\phi_w \qquad (23)\\
< S_x^2\ S_y^2 > &= \frac{1}{8}\left[< S_u^4 > +2 < S_u^2\ S_c^2 > + < S_c^4 >\right] \\
&\quad -\frac{1}{8}\left[< S_u^4 > -6 < S_u^2\ S_c^2 > + < S_c^4 >\right]\cos 4\phi_w \qquad (24)\\
< S_x\ S_y^3 > &= -\frac{1}{4}\left[< S_u^4 > - < S_c^4 >\right]\sin 2\phi_w \\
&\quad +\frac{1}{8}\left[< S_u^4 > -6 < S_u^2\ S_c^2 > + < S_c^4 >\right]\sin 4\phi_w \qquad (25)\\
< S_x^4 > &= \frac{3}{8}\left[< S_u^4 > +2\ < S_u^2\ S_c^2 > + < S_c^4 >\right] \\
&\quad -\frac{1}{2}\left[< S_u^4 > - < S_c^4 >\right]\cos 2\phi_w \\
&\quad +\frac{1}{8}\left[< S_u^4 > -6\ < S_u^2\ S_c^2 > + < S_c^4 >\right]\cos 4\phi_w \qquad (26)
\end{aligned}
$$

Noting that for a Gaussian process, $< S_u^4 >= 3\ < S_u^2 >$, $< S_c^4 >= 3\ < S_c^2 >$ and $< S_u^2\ S_c^2 >=< S_u^2 >< S_c^2 >$, the following form for the PO theory is obtained:

$$
\begin{aligned}
\Delta T_\zeta^{PO,(4)} &\approx -T_s\left(\begin{bmatrix} \frac{1}{64}S_1^4\left[g^{PO}_{\zeta,(\alpha)^4} + g^{PO}_{\zeta,(\beta)^4} + 2\ g^{PO}_{\zeta,(\alpha)^2,(\beta)^2}\right] \\ 0 \end{bmatrix}\right. \\
&\quad + \begin{bmatrix} \frac{1}{16}S_2^4\left[g^{PO}_{\zeta,(\alpha)^4} - g^{PO}_{\zeta,(\beta)^4}\right]\cos(2\phi_w) \\ -\frac{1}{8}S_2^4\left[g^{PO}_{\zeta,(\alpha)^3,\beta} + g^{PO}_{\zeta,\alpha,(\beta)^3}\right]\sin(2\phi_w) \end{bmatrix} \\
&\quad \left. + \begin{bmatrix} \frac{1}{64}S_3^4\left[g^{PO}_{\zeta,(\alpha)^4} + g^{PO}_{\zeta,(\beta)^4} - 6\ g^{PO}_{\zeta,(\alpha)^2,(\beta)^2}\right]\cos(4\phi_w) \\ -\frac{1}{16}S_3^4\left[g^{PO}_{\zeta,(\alpha)^3,\beta} - g^{PO}_{\zeta,\alpha,(\beta)^3}\right]\sin(4\phi_w) \end{bmatrix}\right) \\
&\approx -T_s\left(S_1^4\ L^{PO,4}_{\zeta,0}(\theta_i,\epsilon) + S_2^4\ L^{PO,4}_{\zeta,2}(\theta_i,\epsilon)\begin{bmatrix}\cos(2\phi_w)\\ \sin(2\phi_w)\end{bmatrix}\right. \\
&\quad \left. + S_3^4\ L^{PO,4}_{\zeta,4}(\theta_i,\epsilon)\begin{bmatrix}\cos(4\phi_w)\\ \sin(4\phi_w)\end{bmatrix}\right) \qquad (27)
\end{aligned}
$$

The final form obtained is identical to Equation (19), except for the use of $L^{PO,4}_{\zeta,k}$ as opposed to $L^4_{\zeta,k}$. Comparisons between the theories can therefore be performed solely in terms of the long wave functions themselves.

4.3 Comparison of SSA4 and PO theories

A comparison of the long wave functions $L^4_{\zeta,k}$ and $L^{PO,4}_{\zeta,k}$, $\{k = 0, 2, 4\}$, for sea water permitivity $(29.04 + i35.55)$ at 19.35GHz, for h, v, and U polarizations is provided in Figure 1. Both theories predict the long wave function for the fourth Stokes' parameter to vanish. Long wave functions from the two theories are in agreement, indicating that the SSA model continues to match PO to fourth order.

The long wave functions illustrated show similar amplitudes across azimuthal harmonics as well as polarizations, with all tending to show increasing amplitudes as the polar observation angle is increased. Second azimuthal long wave functions tend to have slightly larger amplitudes. Again these functions are scaled by the appropriate slope moments when computing brightness contributions; as discussed previously, the expected size of these slope moments results in small fourth azimuthal harmonic contributions as compared to the zeroth and second azimuthal harmonics.

5 "Interaction" effects among long and short sea waves

While a direct numerical computation of the four-fold integration of Equation (14) is possible, such computations yield little insight into the emission physics captured by the SSA4 model. Because all limits on the integrations of Equation (14) are infinite, such a computation includes interactions among all possible sea waves, including "long-long" (PO limit), "long-short", and "short-short". However the focus of the current paper is an examination of "long-short" interactions in order to assess a description of these interactions as "tilt" effects (as in the two-scale theory.) The process begins in Section 5.1 by identifying the portion of the integration region relevant for this purpose, and "critical phenomenon" behaviors of the SSA4 kernels are discussed in Section 5.2. A numerical integration scheme that is applicable to computation of the four-fold integral in this portion of the integration domain in then developed in Section 5.3. Description of an approximation to simplify the computations then follows in Section 6, along with interpretation of the results of this expansion.

5.1 Symmetrization of the SSA4 integration

To allow clear identification of "long-short" wave interactions in the four-dimensional integration domain, symmetry properties of the integrands are first applied to reduce this domain. Because the surface spectra involved in the integration by definition must be symmetric under the negation of both arguments, and also due to the "interchange" symmetric form (i.e. $(k_x, k_y) \leftrightarrow (k'_x, k'_y)$) of the product of two spectra involved, it is possible to consider 8 symmetric regions in the integrand of Equation (14). Using a symmetrization process based on these properties, a symmetrized kernel can be defined as

$$\begin{aligned} g_\zeta^{T,(4),sym}(k_x, k_y, k'_x, k'_y) = \Big\{ & g_\zeta^{T,(4),shf}(k_x, k_y, k'_x, k'_y) \\ & + g_\zeta^{T,(4),shf}(-k_x, -k_y, k'_x, k'_y) + g_\zeta^{T,(4),shf}(k_x, k_y, -k'_x, -k'_y) \\ & + g_\zeta^{T,(4),shf}(-k_x, -k_y, -k'_x, -k'_y) + g_\zeta^{T,(4),shf}(k'_x, k'_y, k_x, k_y) \\ & + g_\zeta^{T,(4),shf}(-k'_x, -k'_y, k_x, k_y) + g_\zeta^{T,(4),shf}(k'_x, k'_y, -k_x, -k_y) \\ & + g_\zeta^{T,(4),shf}(-k'_x, -k'_y, -k_x, -k_y) \Big\} \end{aligned} \tag{28}$$

Under this symmetrization, the integration domain can be reduced to the region

$$k'_x > k_x > 0 \tag{29}$$

as illustrated in Figure 2(a) for $k_x = k_c$. If the coordinates (k'_x, k'_y) are now chosen to represent a "short wave" and (k_x, k_y) to represent a "long" wave, the portions of the domain corresponding to long-short wave interactions are as illustrated in Figure 2(b), where k_c refers to the maximum wavenumber of the long wave region. The integration regions in the long and short wave planes are approximated as annular regions in these two planes for convenience. The quantity k_c is chosen to be much less than the electromagnetic wavenumber to ensure only "long" waves are considered in the (k_x, k_y) plane, while the inner radius of the annulus in the (k'_x, k'_y) plane is chosen to be $>> k_c$ to ensure that "short" waves are modeled here. For the purposes of the expansion to be introduced later, "short" actually refers simply to short relative to the shortest "long" sea wave, rather than short relative to the electromagnetic wavelength.

In polar coordinates, Equation (14) can now be expressed on the defined integration domain as two coupled double integrals:

$$\begin{aligned} \Delta T_{\zeta}^{(4)} &= -T_s \int k_\rho \, dk_\rho \int d\phi \; W(k_\rho, \phi) \; \hat{g}(k_\rho, \phi) \\ \hat{g}(k_\rho, \phi) &= \int k_{\rho'} \, dk_{\rho'} \int d\phi' \; W(k_{\rho'}, \phi') \; g(k_\rho, \phi, k_{\rho'}, \phi') \end{aligned} \tag{30}$$

where the superscripts on the symmetrized kernel function are dropped; this kernel is to be used in all following discussions. The outer integration of Equation (30) is evaluated on the long wave plane, while the inner integration is evaluated on the short wave plane.

5.2 Critical phenomena in SSA4 kernels

It is well known that both the second and third order SSA emission kernels exhibit rapid variations (singular-like) behaviors on circular regions in their integration domains. These behaviors are called "critical phenomena" in the literature, and their presence requires numerical integrations involving the SSA kernels to be performed carefully. Because such variations are also likely in the fourth order SSA kernel, a study of the SSA4 kernel functions was performed to identify critical phenomenon behaviors and their locations in the domain of interest. This analysis showed that for a fixed point in the long wave plane, rapid variations in the kernels occurred in the vicinity of six distinct circles in the short wave plane. Tests varying the long wave point considered showed that these circles can be expressed in terms of (k_x, k_y) and (k'_x, k'_y) as:

$$\begin{aligned} (k'_x \pm k_{xi})^2 + (k'_y)^2 &= (k_o)^2 \\ (k'_x + k_x \pm k_{xi})^2 + (k'_y + k_y)^2 &= (k_o)^2 \\ (k'_x - k_x \pm k_{xi})^2 + (k'_y - k_y)^2 &= (k_o)^2 \end{aligned} \tag{31}$$

Here k_o is the electromagnetic wavenumber and $k_{xi} = k_o \sin(\theta_i)$. The first pair of circles do not depend on the long wave coordinates, and can be considered "fixed singular circles" as the long wave coordinates are varied. These are the same singular locations obtained in the second order SSA emission kernels. The other four circles involve the long wave coordinates (i.e. they move inside the short wave plane as the point in the long wave plane moves) and are called "moving

singular circles". Typically in the following presentations, the short wave plane will be discussed after fixing a reference point in the long wave plane.

An illustration of typical critical phenomenon behaviors of the SSA4 kernel functions is provided in Figures 3, 4, and 5, using a radiometer polar observation angle of 55 degrees and a medium relative permittivity of $\epsilon = 29.04 + i35.55$.

Plot (a) of Figure 3 illustrates a particular long wave point given as $(k_\rho, \phi) = (\frac{k_\rho}{4}, \frac{\pi}{6})$, and includes an illustration of the typical integration region boundaries (dashed lines) considered in long-short wave computations; the cutoff wavenumber (largest value of the k_ρ) is specified as $k_c = \frac{k_\rho}{2}$ here. These wavenumber choices are larger than would usually be used in order to emphasize distances between the multiple circles in the short-wave plane.

Plot (b) of Figure 3 illustrates the short wave plane, again with typical boundaries of the integration region marked as dashed lines. Critical phenomenon circles are also included in the plot. A line segment (thicker line) is also included in Figure 3; values of the kernel functions are examined along this line in Figures 4 and 5. Intersections of the line considered with the critical phenomenon circles are numbered from (1) to (3).

Figure 4 plots SSA4 kernel functions for all four polarimetric quantities (here VV refers to the fourth Stokes' parameter) on the line segment of Figure 3(b). Figure 5 zooms in on these functions near the intersection points, and normalizes the curves to their maximum in Figure 4. The results show the rapid variations of the kernels to be confined to relatively small regions near the circular intersections; outside these regions the SSA4 kernels are relatively smooth. Note unlike the second order SSA kernels, the fourth order critical phenomenon behaviors typically show both large positive and negative values (as in the vertical polarization kernel near point (1) compared to point (2) in Figure 5.) Therefore the critical phenomenon contributions tend to cancel out when the integration over the line segment is performed. Notice also that as the long-wave point considered is varied from the $(k_\rho, \phi) = (\frac{k_\rho}{4}, \frac{\pi}{6})$ value used to Figures 3-5, the locations of the intersections (1) to (3) vary. In particular, as the long wave is made longer (i.e. closer to the origin of the long wave plane), the intersections (1) and (3) move closer to the point (2), resulting in large positive

and negative values of the kernel functions both being obtained near the point (2). These rapid variations make numerical computation of long-short wave interactions difficult. The next section presents a numerical integration method suited for these computations.

5.3 Numerical integration of long-short wave interaction contributions

Numerical integration of the SSA4 kernels can be simplified by dividing the full domain integration into piece-wise integrations between intersections with the critical phenomenon circles. For this purpose, a notation for the boundaries of these piece-wise integrations in the $k_{\rho'}$ and ϕ' variables of the short wave plane is introduced.

The set of $k_{\rho'}$ boundaries are defined as $k_{\rho,l}$ with $l = 0, 1, 2, \cdots, l_{max}$, with $k_{\rho,0}$ marking the lower boundary of the entire $k_{\rho'}$ integration and $k_{\rho,l_{max}}$ marking the outer boundary. Similarly, for a given value of l, integration boundaries in the ϕ' variable are written as the set $\phi_{l,m}$ for $m = 0, 1, 2, \cdots, m_{max(l)}$. Here $\phi_{l,0}$ and $\phi_{l,m_{max(l)}}$ mark the lower and upper boundaries of the ϕ' integration. Intermediate values of $\phi_{l,m}$ mark intersections with the critical phenomenon circles, as well as "buffer" points surrounding these intersections by a specified separation in ϕ'. Because the ϕ' integration is performed first, intermediate values of $k_{\rho,l}$ were chosen based on intersections with the critical phenomenon circles for $\phi' = 0$, again with "buffer" points surrounding these boundaries included in the set of points.

Using these definitions, the short wave integral of Equation (30) can be rewritten as:

$$\hat{g}(k_\rho, \phi) = \sum_{l=1}^{l_{max}} \int_{k_{\rho,l-1}}^{k_{\rho,l}} k_{\rho'}\, dk_{\rho'} \sum_{m=1}^{m_{max(l)}} \int_{\phi_{m-1}}^{\phi_m} d\phi'\, W(k_{\rho'}, \phi')\, g(k_\rho, \phi, k_{\rho'}, \phi') \tag{32}$$

Note it is also possible to reverse the order of these integrations by redefining the piece-wise limits first in terms of $k_{\rho'}$ then in terms of ϕ'; both approaches were evaluated and found to perform similarly.

The piece-wise integrations of Equation (32) now involve relatively smooth functions because the regions of rapid kernel variations are automatically resolved. Accordingly, a standard Gauss-Legendre quadrature is applied both in ϕ' and in $k_{\rho'}$ for computation of each of the piece-wise two-fold integrals.

Given this process for evaluating the short-wave plane integration, it remains to evaluate the integration over the long-wave plane. This integration is less numerically challenging because the short-wave integration smooths out kernel function variations. Therefore a standard Gauss-Legendre quadrature is applied for the k_ρ and ϕ integrations without further treatment.

Numerous tests of this approach were performed to ensure that a sufficient number of quadrature points, etc. was utilized to obtain convergence of model predictions. Results using the method described showed that convergence was obtained with use of only a moderate number (order to 100) quadrature points within each piece-wise integration. Because even a single evaluation of the symmetrized SSA4 kernel function is a relatively expensive operation, codes were developed to compute and output a table of these kernels over the integration domain. These tables then allow more efficient computations of fourth order emission predictions as properties of the sea spectrum (for example, wind speed) are varied. Results from the numerical integration of long-short wave contributions will be discussed in Section 7, and compared with the approximation of long-short wave contributions defined in the next Section.

6 Approximations for long-short wave contributions

6.1 Long-wave expansion of SSA4 short-wave integrations

Due to the rapidly varying nature of the SSA4 kernel functions and the presence of the "moving singular circles" in the short wave plane, extreme care must be exercised when attempting to expand the SSA4 kernel functions in terms of long wave parameters. To address this issue, expansion of the result of the short wave integration is first considered before proceeding to expansion of the SSA4 kernel functions themselves.

Based on the slope expansion implicit in the SSA4 theory, it is to be expected that an expansion of the $\hat{g}(k_x, k_y)$ quantity in terms of k_x and k_y should be applicable near the origin (i.e. very long long waves); the return to rectangular wavenumber coordinates is made for convenience in what follows. It is also to be expected that the zeroth and first order terms in such an expansion will

vanish, leaving

$$\hat{g}(k_x, k_y) \approx \frac{k_x^2}{2}\ \hat{g}_{k_x^2}(0,0) + \frac{k_y^2}{2}\ \hat{g}_{k_y^2}(0,0) \tag{33}$$

The subscripts k_x^2 and k_y^2 again represent second partial derivatives with respect to k_x and k_y, and the cross $k_x k_y$ term is found to vanish when it is assumed that the radiometer observes along the x axis of the coordinate system. With this expansion, the fourth order brightness contribution reduces to

$$\Delta T^{(4)} \approx \frac{-T_s}{2}\left[< S_x^2 > \hat{g}_{k_x^2}(0,0) + < S_y^2 > \hat{g}_{k_y^2}(0,0)\right] \tag{34}$$

where $< S_x^2 >$ and $< S_y^2 >$ are the along- and cross-look slope variances of the long waves considered. This form is attractive for evaluating long-short wave contributions due to its efficiency when compared to the four-fold integration. Note this expansion is performed following the integration over the short-wave plane, so that the derivatives considered depend on the short wave spectrum.

Numerical tests using a centered difference algorithm for the Taylor expansion of $\hat{g}(k_x, k_y)$ near the origin confirmed that the zeroth and first order terms vanish. The remaining second order derivatives were computed as

$$\hat{g}_{k_x^2}(0,0) = \lim_{h\to 0} \frac{2\ \hat{g}(h,0)}{h^2}, \quad \hat{g}_{k_y^2}(0,0) = \lim_{h\to 0} \frac{2\ \hat{g}(0,h)}{h^2} \tag{35}$$

due to the symmetry properties of $\hat{g}(k_x, k_y)$. The k_x^2 derivative can be more explicitly written as

$$\hat{g}_{k_x^2}(0,0) = \lim_{h\to 0} \int k_{\rho'}\ dk_{\rho'} \int d\phi'\ W(k_{\rho'}, \phi')\ \frac{2\ g(h, 0, k_{\rho'}, \phi')}{h^2} \tag{36}$$

Expressions for k_y^2 derivative are almost identical, and therefore not discussed specifically in what follows. Results from this approach will not be considered further, but were used in verifying the accuracy of the expansion discussed in the next paragraph.

6.2 Long wave expansion of SSA4 kernel functions

A more useful and efficient form of the long-short wave expansion can be obtained by moving the limit operator inside the integrals, so that derivatives of the SSA4 kernels, rather than the result of the short wave plane integration, are involved. The result of such an interchange for the k_x^2 term is

$$\hat{g}_{k_x^2}(0,0) \approx \int k_{\rho'}\ dk_{\rho'} \int d\phi'\ W(k_{\rho'}, \phi')\ g_{k_x^2}(0, 0, k_{\rho'}, \phi') \tag{37}$$

where $g_{k_x^2}(0,0,k_{\rho'},\phi')$ represents the SSA4 kernel derivative $\lim_{h\to 0}\frac{2g(h,0,k_{\rho'},\phi')}{h^2}$.

Equation (37) along with Equation (34) shows $g_{k_x^2}(0,0,k_{\rho'},\phi')$ (and a similar $g_{k_y^2}(0,0,k_{\rho'},\phi')$ term) to be spectrum independent "weighting functions" that describe contributions of a particular short wave $(k_{\rho'},\phi')$ to the total long-short wave brightness when multiplied by the long wave slope variance. This form approximates the tilting process, and is therefore relevant for use in comparisons with the two-scale theory. In such a comparison, the original two-scale model equations can be expanded into a similar series in long-wave slopes; results show the zeroth order term to be that of a flat surface, the second order term to be identical to the second order small slope theory, and the fourth order term to be identical to Equation (34) except that two-scale model derivatives $g_{k_x^2}^{two}(0,0,k_{\rho'},\phi')$ are involved as opposed to those from the SSA4. Therefore sea spectrum independent comparisons of the two theories and their predictions of long-short wave tilt effects can be performed in terms of the kernel function derivatives alone.

Because the SSA4 kernels are not truly singular, the required expansion of the SSA4 kernels is possible, but remains numerically difficult due to critical phenomenon effects. The h dependence of the $k_{\rho'}$ and ϕ' grids in the short wave plane further complicates this process. Although this dependence should vanish identically as $h\to 0$, the effects of finite h values in finite precision computations remain observable particularly near the critical phenomenon regions. For this reason, the weighting functions to be illustrated should be considered only "semi-stable" representations, with some degree of h dependence remaining. However it is again emphasized that the extreme SSA4 kernel function values obtained near the critical phenomenon regions largely cancel out when integrated, so that the effect of this "semi-stable" nature is not significant when computing final fourth order brightnesses. Evidence supporting this statement will be provided in Section 7 through comparisons with numerically integrated long-short wave contributions.

Further simplification of the final fourth order brightness in this approximation can be obtained by substituting an assumed form for the sea spectrum:

$$W(k_\rho,\phi)=\frac{1}{k_\rho^4}\left[C_0(k_\rho)+C_2(k_\rho)\cos\left(2\left(\phi-\phi_w\right)\right)\right] \tag{38}$$

with ϕ_w representing the wind direction; it is assumed that the radiometer look direction is along

x in what follows (i.e. the azimuthal angle of the radiometer observation direction is zero). The fourth order brightness is then

$$\Delta T_\zeta^{(4)} \approx \frac{-T_s}{2}\left(< S_x^2 > \int dk_{\rho'} \begin{bmatrix} C_0(k_{\rho'}) \\ C_2(k_{\rho'}) \end{bmatrix}^T \int d\phi' \begin{bmatrix} 1 \\ \cos(2\,(\phi' - \phi_w)) \end{bmatrix} \frac{g_{k_x^2}(0,0,k_{\rho'},\phi')}{k_{\rho'}^3} + < S_y^2 > \int dk_{\rho'} \begin{bmatrix} C_0(k_{\rho'}) \\ C_2(k_{\rho'}) \end{bmatrix}^T \int d\phi' \begin{bmatrix} 1 \\ \cos(2\,(\phi' - \phi_w)) \end{bmatrix} \frac{g_{k_y^2}(0,0,k_{\rho'},\phi')}{k_{\rho'}^3} \right) \quad (39)$$

This expression is valid in general, but, in order to extract the azimuthal harmonics in wind direction, it is more convenient to expand the original multiplication of long and short wave spectra into terms involving $[1, \cos(2\phi_w), \sin(2\phi_w), \cos(4\phi_w), \sin(4\phi_w)]$ as follows:

$$\begin{aligned} k_\rho^4 k_{\rho'}^4 W(k_\rho,\phi) W(k_{\rho'},\phi') = & \left[\left(C_0(k_\rho)C_0(k_{\rho'}) + \frac{1}{2} C_2(k_\rho)C_2(k_{\rho'}) \cos(2\,(\phi - \phi')) \right) + \right. \\ & \left(C_0(k_\rho)C_2(k_{\rho'}) \cos(2\phi') + C_2(k_\rho)C_0(k_{\rho'}) \cos(2\phi) \right) \cos(\mathbf{2}\phi_\mathbf{w}) + \\ & \left(C_0(k_\rho)C_2(k_{\rho'}) \sin(2\phi') + C_2(k_\rho)C_0(k_{\rho'}) \sin(2\phi) \right) \sin(\mathbf{2}\phi_\mathbf{w}) + \\ & \left(\frac{1}{2} C_2(k_\rho)C_2(k_{\rho'}) \cos(2\,(\phi + \phi')) \right) \cos(\mathbf{4}\phi_\mathbf{w}) + \\ & \left. \left(\frac{1}{2} C_2(k_\rho)C_2(k_{\rho'}) \sin(2\,(\phi + \phi')) \right) \sin(\mathbf{4}\phi_\mathbf{w}) \right] \end{aligned} \quad (40)$$

Use of this representation along with expansion of the sinusoidal terms in $\phi + \phi'$ and $\phi - \phi'$ allows a combination of terms to be defined for determining a specific azimuthal harmonic of the observed brightnesses.

The result of the ϕ' integration of individual terms in this combination is defined through

$$w_{\zeta,(x,y)}^{(1,c,s)}(k_{\rho'}) = \int d\phi' \begin{bmatrix} 1 \\ \cos(2\phi') \\ \sin(2\phi') \end{bmatrix} \frac{g_{\zeta,k_{(x,y)}^2}(0,0,k_{\rho'},\phi')}{k_{\rho'}^3} \quad (41)$$

and denoted as a "weighting function" in what follows. It is these weighting functions that can be compared with similar weighting functions from the expanded two-scale theory. Here the subscript ζ represents the polarization, the subscripts (x, y) represent either the second order x or y derivative, and the superscripts $(1, c, s)$ represent use of either constant, $\cos(2\phi')$, or $\sin(2\phi')$ factors in the ϕ' integration.

Finally, harmonics of the fourth order brightness contribution are written using the weighting

functions defined above as

$$\begin{aligned} H_{\zeta}^{(0)} &= -\frac{\pi}{4}T_s\left[I_0\int dk_{\rho'}C_0(k_{\rho'})\left(w_{\zeta,(x)}^{(1)}(k_{\rho'})+w_{\zeta,(y)}^{(1)}(k_{\rho'})\right)\right. \\ &\quad \left.+\frac{I_2}{4}\int dk_{\rho'}C_2(k_{\rho'})\left(w_{\zeta,(x)}^{(c)}(k_{\rho'})-w_{\zeta,(y)}^{(c)}(k_{\rho'})\right)\right] \\ H_{\zeta}^{(2)} &= -\frac{\pi}{4}T_s\left[I_0\int dk_{\rho'}C_2(k_{\rho'})\left(w_{\zeta,(x)}^{(c)}(k_{\rho'})+w_{\zeta,(y)}^{(c)}(k_{\rho'})\right)\right. \\ &\quad \left.+\frac{I_2}{2}\int dk_{\rho'}C_0(k_{\rho'})\left(w_{\zeta,(x)}^{(1)}(k_{\rho'})-w_{\zeta,(y)}^{(1)}(k_{\rho'})\right)\right] \end{aligned} \tag{42}$$

which applies to the linearly polarized channels. Here $H^{(0)}$ represents the zeroth harmonic, and $H^{(2)}$ represents the second azimuthal harmonic; fourth harmonics are small and not considered further in what follows. For the third and fourth Stokes' parameters, the zeroth harmonic vanishes and the second harmonic is obtained through

$$H_{\zeta}^{(2)} = -\frac{\pi}{4}T_sI_0\int dk_{\rho'}C_2(k_{\rho'})\left(w_{\zeta,(x)}^{(s)}(k_{\rho'})+w_{\zeta,(y)}^{(s)}(k_{\rho'})\right) \tag{43}$$

In the above equations, the terms $I_{(0,2)}$ are defined through

$$I_{(0,2)} = \int dk_{\rho}\frac{C_{(0,2)}(k_{\rho})}{k_{\rho}} \tag{44}$$

with the integration evaluated on long wave domain.

The preceeding equations show that the expanded SSA4 model expresses "long-short" interaction effects in terms of an integration of a combination of the weighting functions defined in equation (41) multiplied by the short wave curvature spectrum. The result of this integration is multiplied by a function resembling the long wave slope variance. Therefore the weighting functions provide sea-surface-independent insight into the relative contributions of particular short scale sea waves to the total observed "long-short" interaction brightnesses.

6.3 Comparison of SSA4 and Two-scale weighting functions

Figures 6 and 7 present comparison of the SSA4 and two-scale "semi-stable" weighting functions for radiometer polar observation angle 55 degrees and $\epsilon = 29.04 + i35.55$. Plots of the zeroth azimuthal harmonic weighting function $w_{h,(x)}^{(1)}(k_{\rho'})$ (horizontal polarization) in Figure 6 include additional plots that provide higher resolution near the critical phenomenon regions marked as (1)

through (3), while Figure 7 illustrates the zeroth azimuthal harmonic weighting function for vertical polarization and the second azimuthal harmonic weighting functions for third and fourth Stokes' parameters without further detail. The figures illustrate weighting function magnitudes, and also include plots of the signs (shifted by 5 units for the multiple curves for convenience).

The weighting functions in Figure 6 are very different near the critical phenomena regions, with the SSA4 kernels showing much larger variations than two scale; note the rapid nulling behavior observed in both SSA4 and two-scale weighting functions results on sign changes of the weighting functions due to the use of a logarithmic vertical axis. However such rapid variations are not expected to make significant brightness contributions due to cancellation effects discussed previously.

Overall the comparison of the SSA4 and two-scale weighting functions shows the two to have similar properties, both in magnitude and signs, particularly in regions far from the critical phenomenon boundaries. However even in such regions, differences between the two models are observed, so that a complete agreement between the two theories is not achieved. Because development of a simple description of the differences between the two weighting functions is not easily obtained, more concrete examples of comparisons with two-scale theory predictions are provided in the next Section.

7 Comparisons of numerically integrated, expanded, and two-scale long-short wave brightness contributions

Numerically integrated (Section 5.3), expanded (Section 6.2), and two-scale model predictions of the azimuthal harmonics of the fourth order long-short wave brightness contributions are compared in this Section. The radiometer frequency is assumed to be 19.35GHz (wavelength $\lambda_o = 1.55$cm, wavenumber $k_o = 405$ rads/m) and a surface relative permitivity $\epsilon = 29.04 + i35.55$ is used. The sea spectrum is modeled using the modified "Durden-Vesecky" spectrum described in [7], and the sea surface physical temperature is set to 283 K. While all theories predict the possibility of zeroth, second, and fourth azimuthal harmonics in this process, fourth azimuthal harmonics are found to be extremely small and therefore not described further. Azimuthal harmonic brightnesses are

plotted either with respect to wind speed (from 0 to 20m/s) for a fixed radiometer observation angle $\theta_i = 55$ degrees, or with respect to observation angle ranging from 40^o to 70^o for a fixed wind speed of 10m/s. In all cases, the boundaries of the short-wave integration correspond to short sea waves of wavelengths ranging from 0.5m down to 4mm.

Two distinct descriptions of the long-wave integration domain are utilized. In the first case (labeled Case A), the long wave domain includes all long waves longer than 62.5 m; the long wave spectrum considered of course varies as the wind speed is varied. In this case, the long waves included are certainly much longer than the short waves of interest, so that the SSA4 expansion should be more applicable. In the second case (Case B), a shorter set of long waves ranging from 62.5 m maximum wavelength down to 0.625 m is used, to assess the applicability of the SSA4 expansion as the separation between "long" and "short" waves is decreased.

Figures 8 (versus wind speed) and 9 (versus angle) plot the comparisons for Case A. First note that the brightness harmonics obtained in Case A are all less than 0.1 K, with the exception of the 0th harmonics at large wind speeds and/or observation angles. This is due to the small rms slopes obtained when only extremely long long waves are included. The wind speed dependence observed arises both from increases in the long wave slope variance considered, but also from changes in the short wave spectrum [7] with windspeed. The comparison among theories shows the SSA4 expansion to be highly accurate in this case when compared to the numerical SSA4 integration, even given the difficulties in evaluation of the kernel function derivatives required in the expansion. Two-scale predictions again are similar to the SSA4 results in terms of general trends and relative amplitudes, but do show observable differences.

Results for Case B in Figures 10 and 11 show larger but still relatively small fourth order effects with maximum amplitudes on the order of 1 K in the zeroth harmonics while remaining less than 0.1 K in second azimuthal harmonics. The expanded SSA4 theory is found to provide reduced accuracy compared to case A, but to still achieve good agreement with the full SSA4 numerical integration. Differences with the two-scale model are more significant, particularly for the zeroth azimuthal harmonic of horizontal polarization, but overall the two-scale model shows similar trends

and amplitudes.

8 Conclusions

Expressions for the fourth-order SSA theory of emission from the sea surface were derived and presented in this paper. For the case of a Gaussian random process surface model, evaluation of the theory requires computation of a four-fold integration over a product of two sea spectra. This form is described as providing information on contributions from interactions of multiple sea waves in the surface spectrum. Predictions of the model were evaluated in two situations: coupling between "long-long" waves and between "long-short" waves. The former contributions were shown to remain consistent with the physical optics theory, as has been previously demonstrated for the second and third order SSA models. "Long-short" wave interactions were studied through the use of a symmetrized kernel function, and by consideration of critical phenomenon effects in the SSA4 kernel functions. A numerical integration procedure for evaluation of "long-short" wave effects was described, as well as an expansion in long wave slopes that yielded a simplified approximation in terms of spectrum independent "weighting functions." A study of these interactions was performed, and it was found that the expansion provided reasonable predictions, even though finite computational precision limited the accuracy of the kernel function derivative evaluation in some cases.

One of the primary goals of the paper was an assessment of the commonly applied "two-scale" theory through comparison with the SSA4. This was performed by comparing the "weighting functions" of the SSA4 expansion with those obtained from a similar expansion of the two-scale theory, as well as through direct comparison of fourth order brightnesses between the theories. Results showed the two methods not to be identical, indicating that the SSA4 model captures long-short wave interactions beyond the simple "tilting" process implicit in the two-scale theory. However studies showed that brightness differences between the two theories were generally small, and can be considered negligible for second azimuthal harmonic variations in particular.

For these reasons, rejection of the two-scale theory in favor of the expanded SSA4 theory does not

appear highly motivated at present. However, the expanded SSA4 theory does produce a reasonably efficient means for evaluating long-short wave interaction effects should further evaluation of this issue be deemed relevant. Further studies using the SSA4 theory to compute "short-short" wave interaction effects may also yield additional motivation for further application of the method.

9 Acknowledgments

This work was supported by the Office of Naval Research, under grant N00014-02-1-0857. Use of supercomputing facilities at the Ohio Supercomputing Center is also acknowledged.

References

[1] Irisov, V. G., "Small-slope expansion for thermal and reflected radiation from a rough surface," *Waves in Random Media,* vol. 7., pp. 1-10, 1997.

[2] Johnson, J. T., and M. Zhang, "Theoretical study of the small slope approximation for ocean polarimetric thermal emission," *IEEE Trans. Geosc. Remote Sens.,* vol. 37, pp. 2305–2316, 1999.

[3] Irisov, V. G., "Azimuthal variations of the microwave radiation from a slightly non-Gaussian sea surface," *Radio Science,* vol. 53, pp. 65–82, 2000.

[4] Johnson, J. T. and Y. Cai, "A theoretical study of sea surface up/down wind brightness temperature differences," *IEEE Trans. Geosc. Remote Sens.,* vol. 40, pp. 66–78, 2002.

[5] Rice, S. O., "Reflection of electromagnetic waves from slightly rough surfaces," *Commun. Pure Appl. Math,* vol. 4, pp. 361–378, 1951.

[6] J. T. Johnson, "Comparison of the physical optics and small slope theories for polarimetric thermal emission from the sea surface," *IEEE Trans. Geosc. Rem. Sens.,* vol. 40, pp. 500–504, 2002.

[7] Yueh, S. H., "Modeling of wind direction signals in polarimetric sea surface brightness temperatures," *IEEE Trans. Geosc. Remote Sens.,* vol. 35, pp. 1400-1418, 1997.

[8] Johnson, J. T., "An efficient two-scale model for the computation of thermal emission and atmospheric reflection from the sea surface," *IEEE Trans. Geosc. Remote Sens.,* March 2006.

[9] Johnson, J. T., "Third order small perturbation method for scattering from dielectric rough surfaces," *J. Opt. Soc. Am. A.,* vol. 16, pp. 2720–2726, 1999.

[10] M. A. Demir, J. T. Johnson "Fourth and higher-order small perturbation solution for scattering from dielectric rough surfaces," *J. Opt. Soc. Am. A*, vol. 20, pp. 2330-2337, 2003.

[11] L. Tsang, J. A. Kong, and R. T. Shin, *Theory of Microwave Remote Sensing,* New York: Wiley-Interscience, 1985.

[12] M. A. Demir, "Fourth order theories of emission and scattering from rough surfaces," M. S. Thesis, Dept. of Electrical and Computer Engineering, The Ohio State University, 2003.

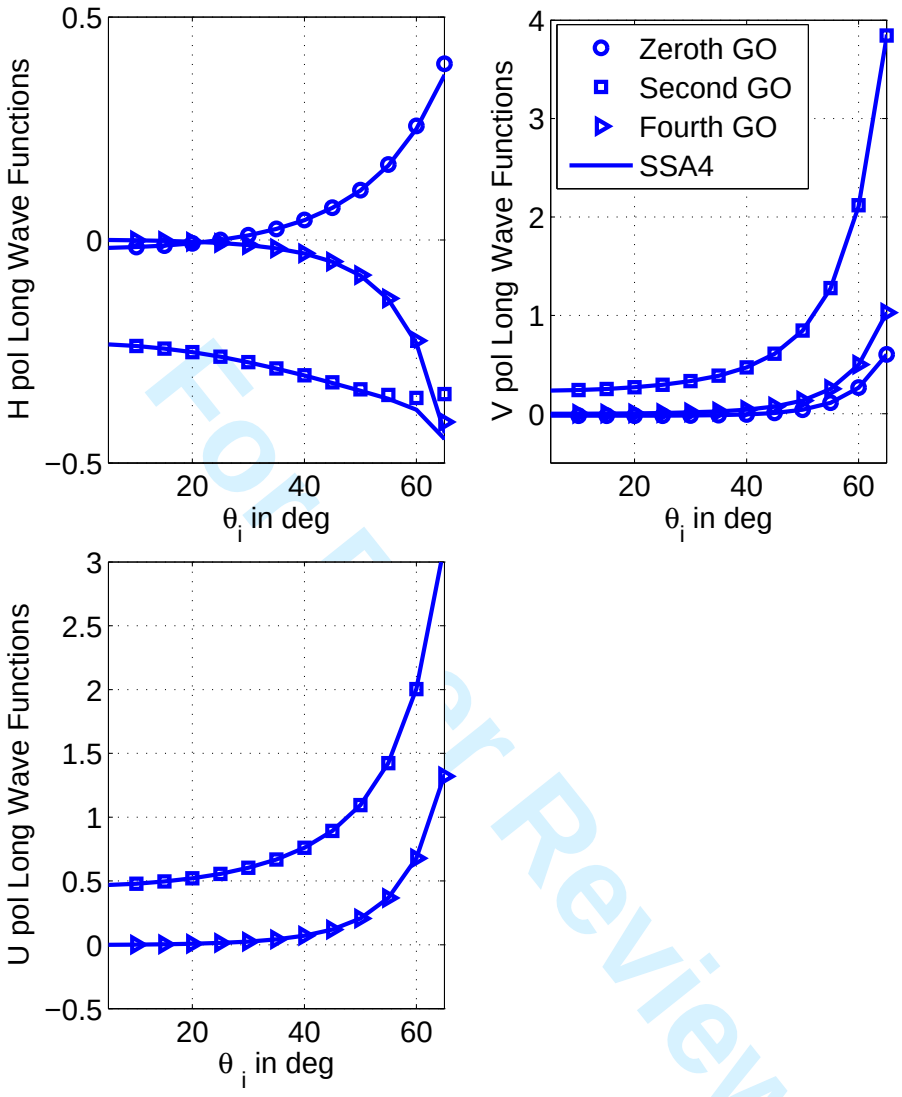

Figure 1: Comparison of the long wave functions $L^4_{\zeta,k}$ and $L^{PO,4}_{\zeta,k}$, $\{k = 0, 2, 4\}$, for sea water permitivity $(29.04 + i35.55)$ at 19.35GHz, for h, v and U polarizations

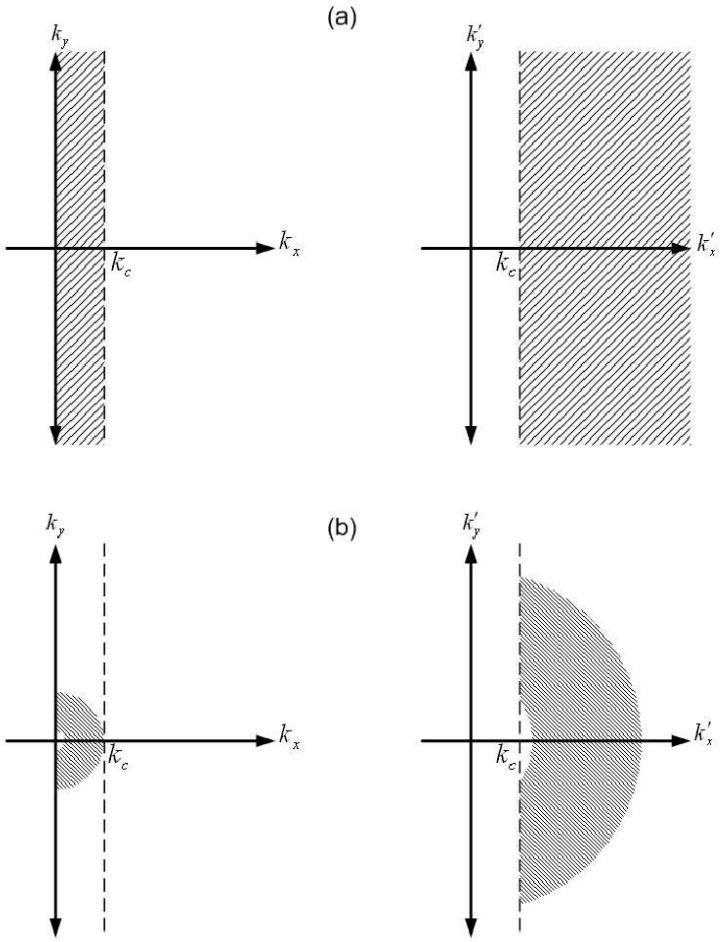

Figure 2: Integration regions (a) Following symmetrization of Equation (14) (b) Reduced integration region for modeling "long-short" sea wave interactions

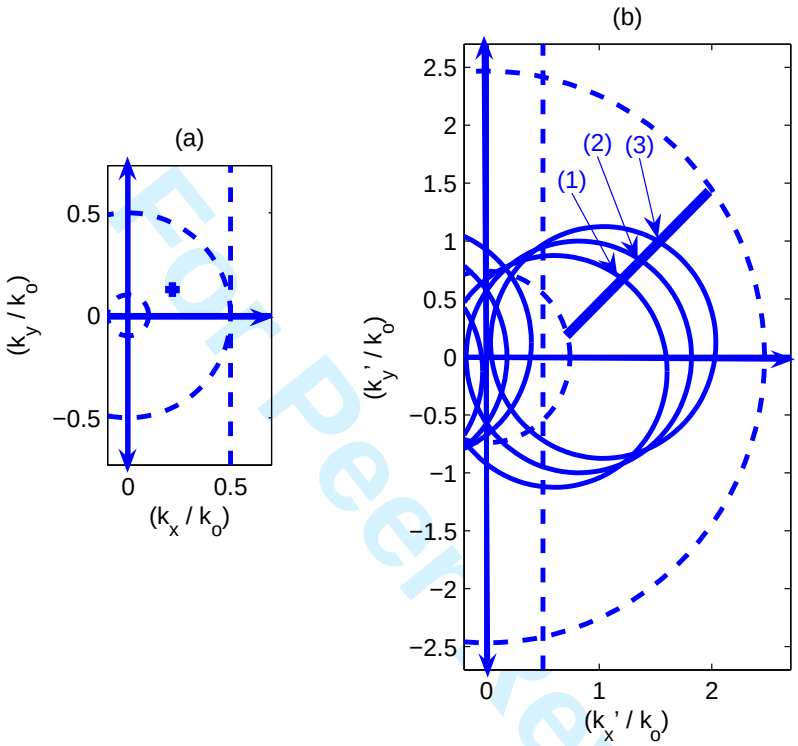

Figure 3: Illustration of critical phenomenon effects, (a)- Long wave domain and a reference point $(k_\rho, \phi) = (\frac{k_o}{4}, \frac{\pi}{6})$, (b)- Short wave domain, domain identifiers (dashed), critical phenomenon circles (solid) and a line segment intersecting the critical phenomenon circles

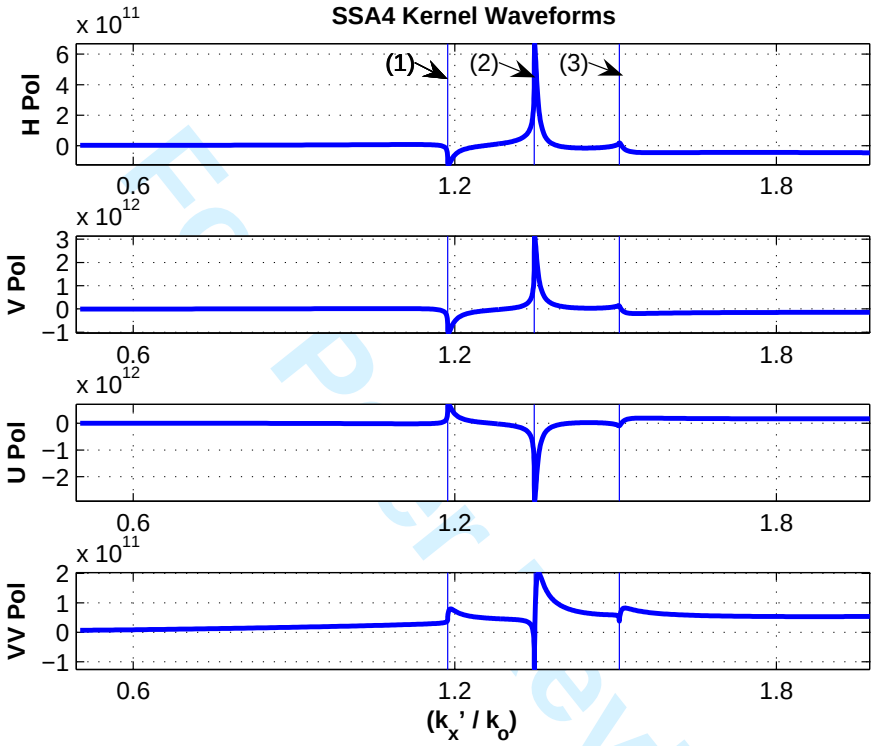

Figure 4: SSA4 kernel waveforms plotted on the line segment of Figure 3.

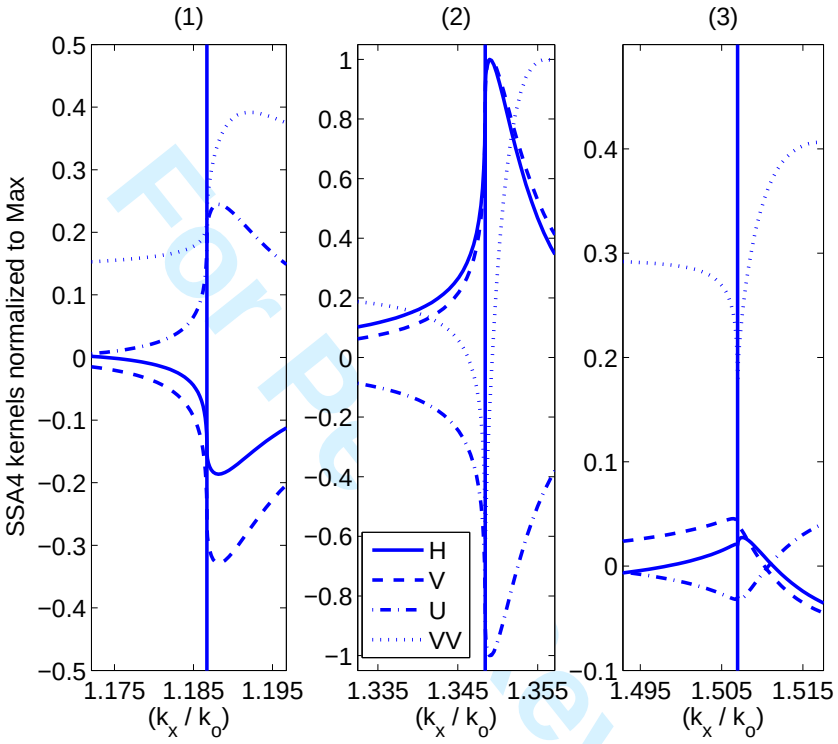

Figure 5: SSA4 kernel waveforms normalized to their maximum values in Figure 3, at the intersection points

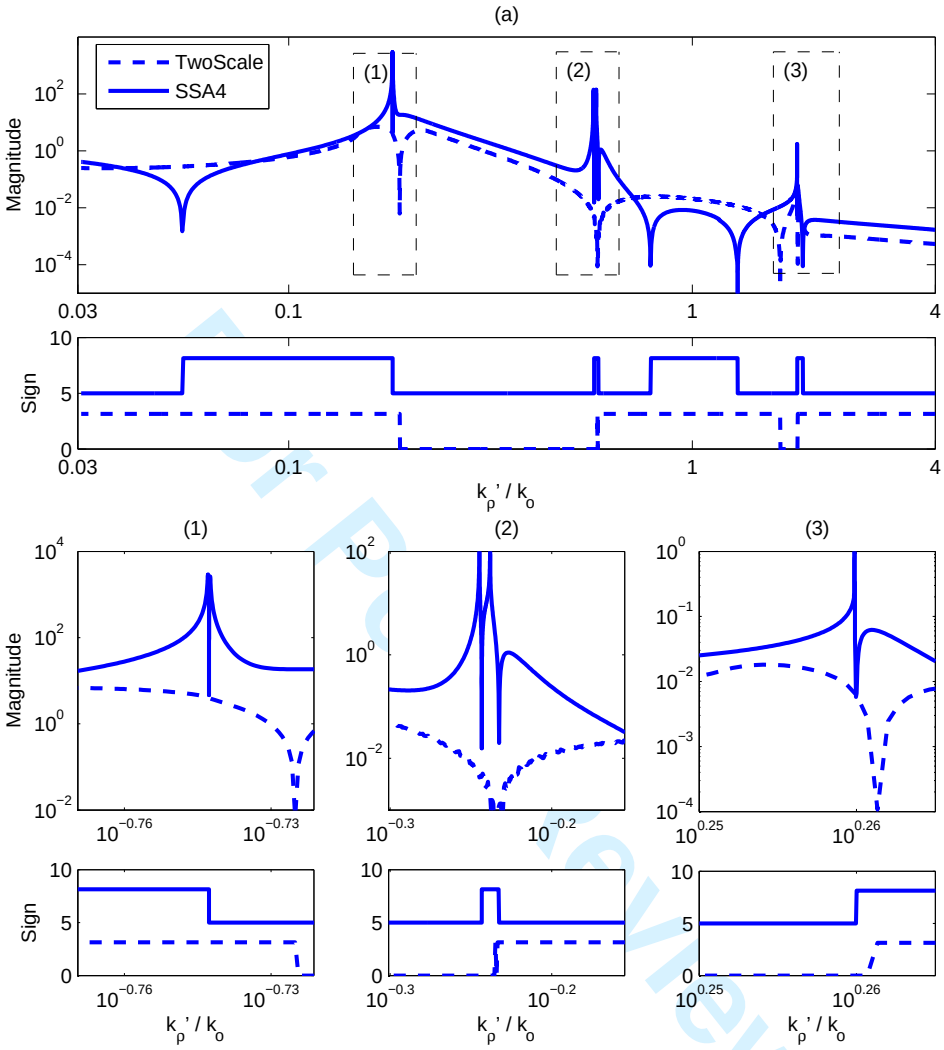

Figure 6: "Semi-stable" horizontally polarized weighting functions $w^{(1)}_{h,(x)}(k_{\rho'})$, including higher resolution plots near critical phenomenon regions (1) to (3)

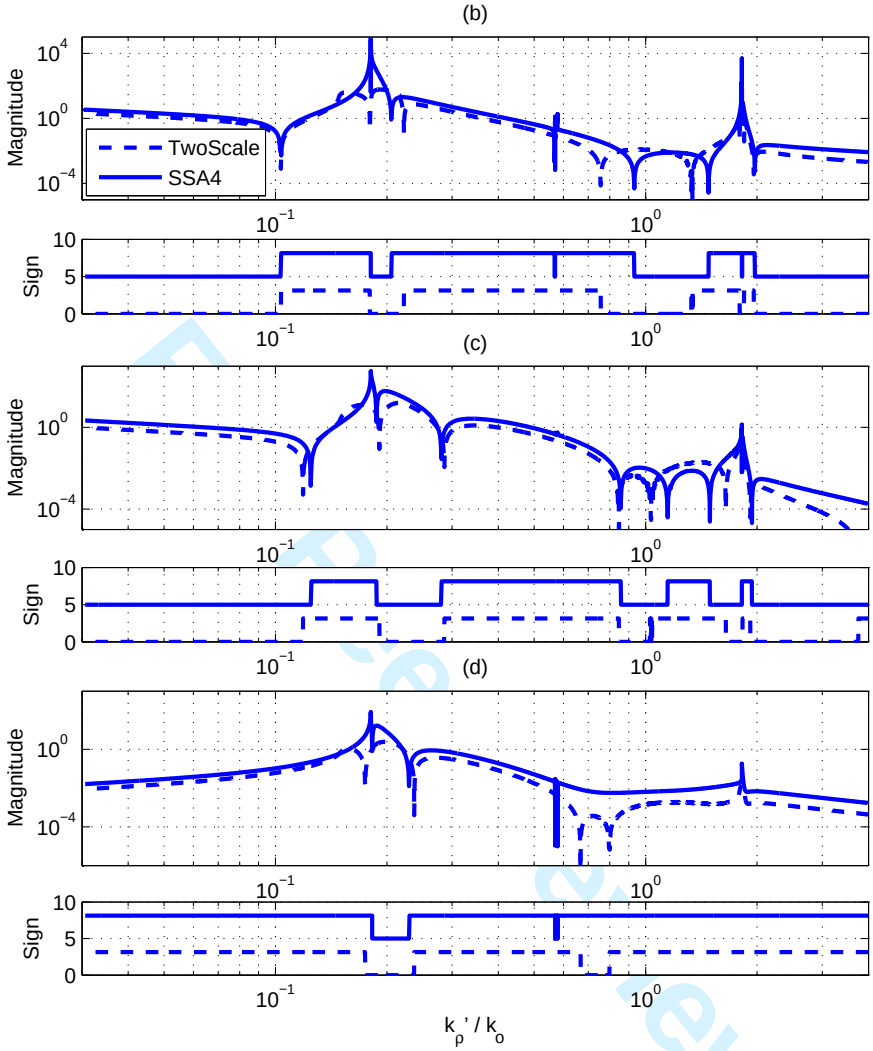

Figure 7: "Semi-stable" weighting functions b)-Vertical Pol.($w^{(1)}_{v,(x)}(k_{\rho'})$) , c)-U pol.($w^{(s)}_{u,(x)}(k_{\rho'})$), d)-VV Pol.($w^{(s)}_{VV,(x)}(k_{\rho'})$)

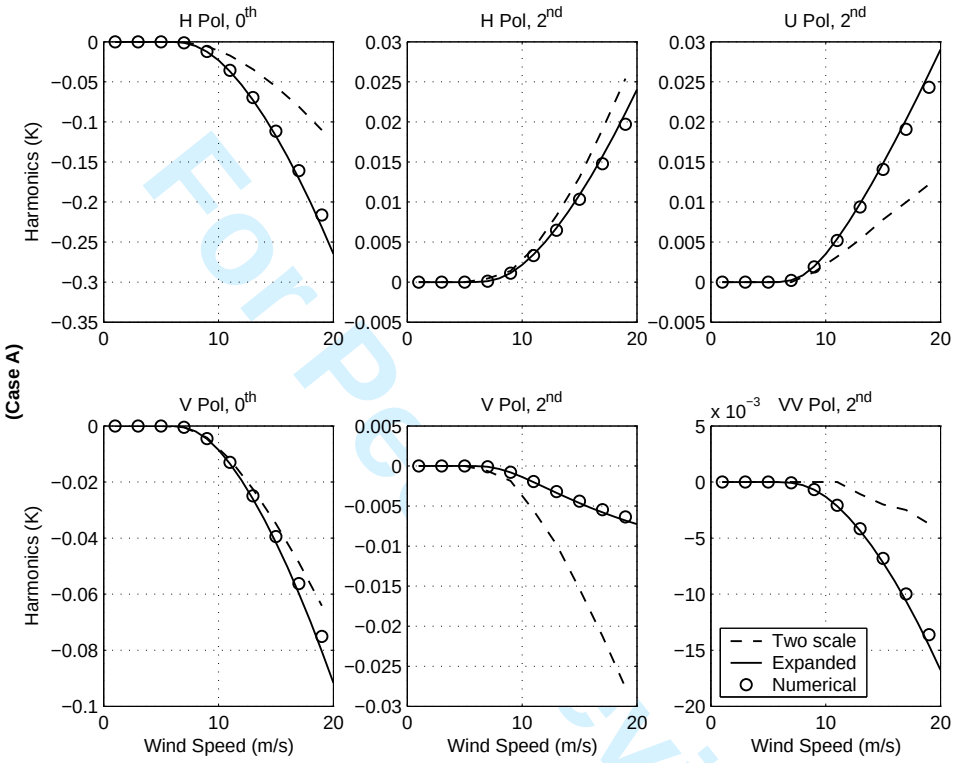

Figure 8: Case A, harmonics versus wind speed

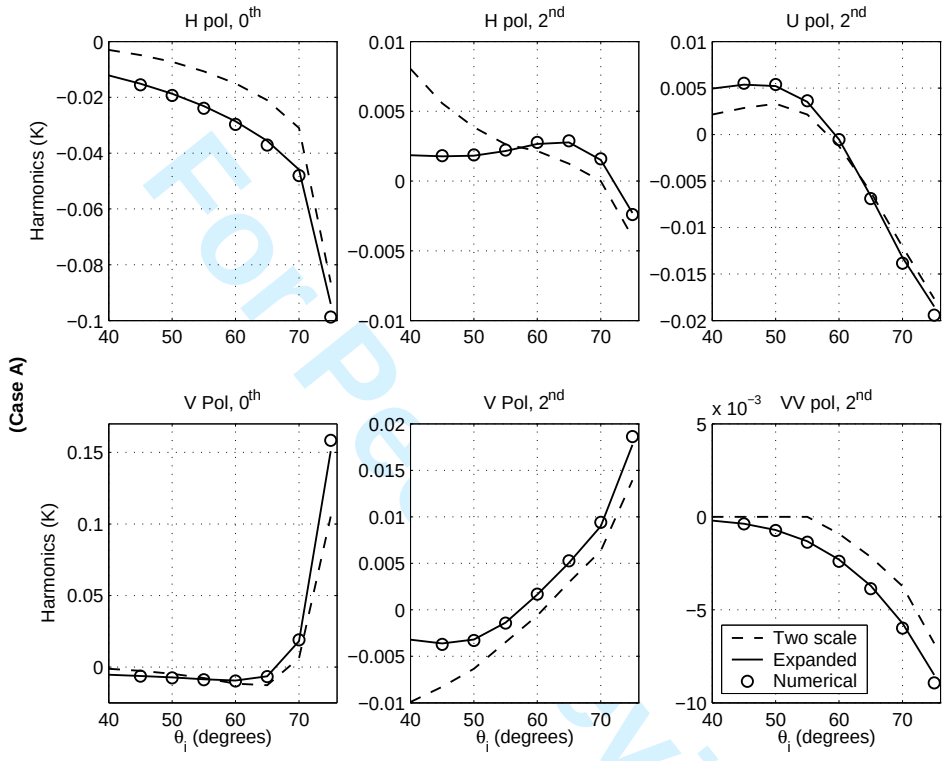

Figure 9: Case A, harmonics versus θ_i

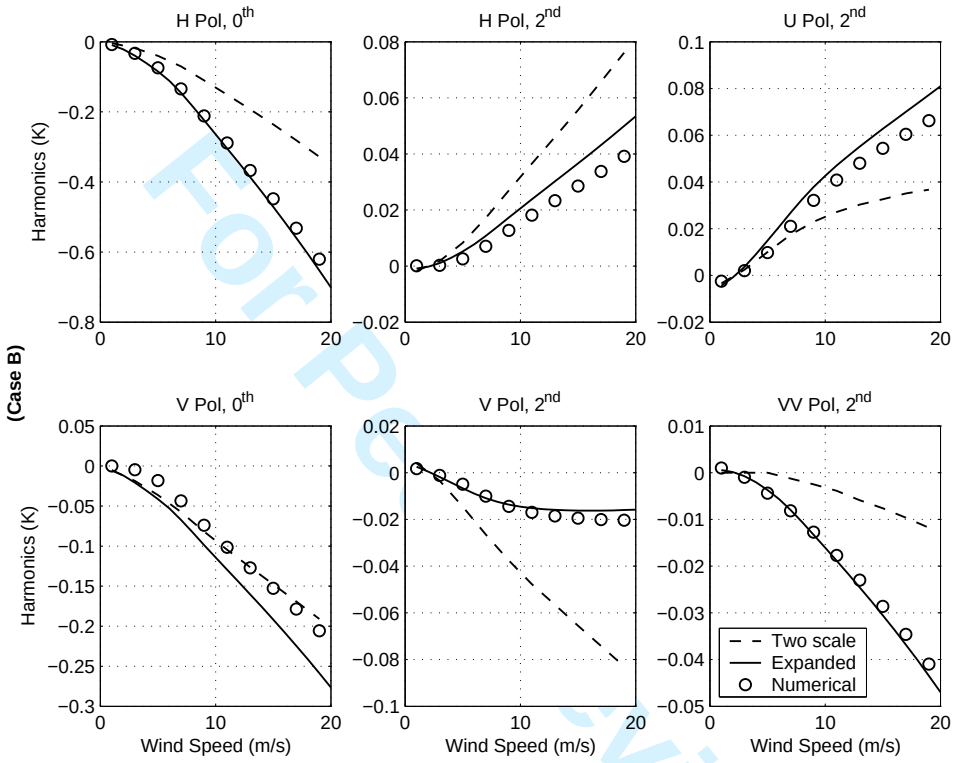

Figure 10: Case B, harmonics versus wind speed

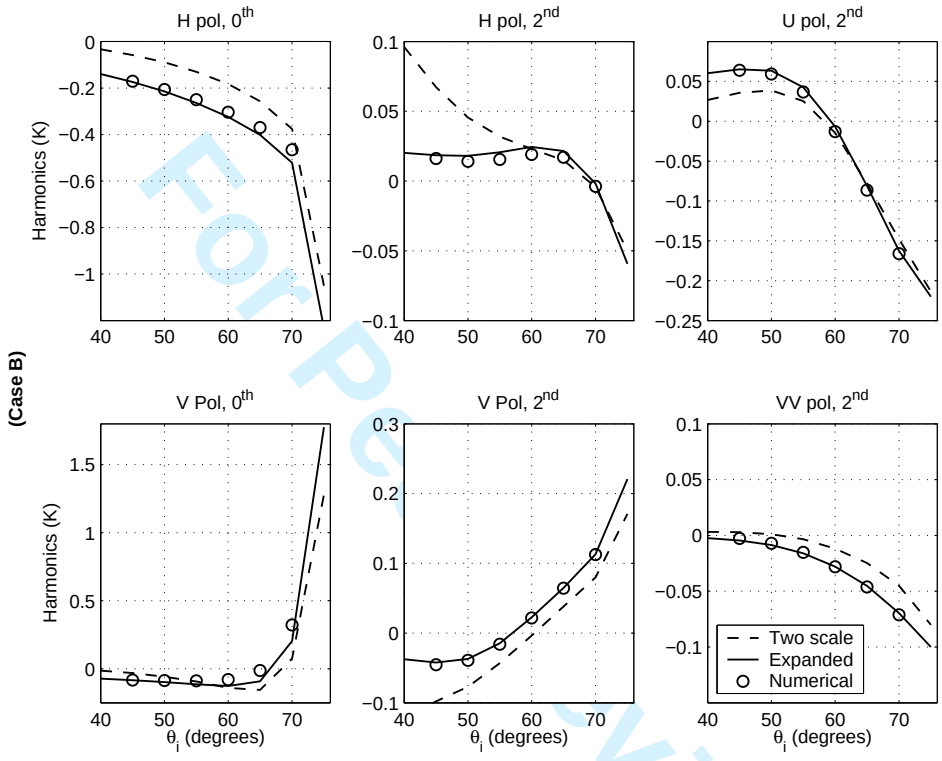

Figure 11: Case B, harmonics versus θ_i